

RESEARCH ARTICLE

Accurate and Resilient GPS-Only Localization With Velocity Constraints

SE-HYOUNG CHO¹, (Member, IEEE), AND SUNGLOK CHOI²¹Information Communications Technology Department, Sun Moon University, Asan-si, Chungcheongnam-do 31460, Republic of Korea²Computer Science and Engineering Department, Seoul National University of Science and Technology (SeoulTech), Nowon-gu, Seoul 01811, Republic of Korea

Corresponding author: Sunglok Choi (sunglok@seoultech.ac.kr)


This work was supported by SeoulTech Internal Research Grant 2021-0899.

ABSTRACT GPS is the most popular sensor for outdoor localization. GPS-only localization is the simplest and initial setting, thus it has been employed in many applications. This paper presents more accurate GPS-only localization with two velocity constraints based on Bayesian filtering. GPS-only localization inherently suffers from ambiguity problems in its state variables due to the limitation of position-only observations. These ambiguities lead to incorrect or diverged state estimates, which are commonly observed in cases of violating assumptions in motion and observation models. Since two proposed velocity constraints can resolve the ambiguity problems, EKF localization with two additional constraints can achieve more accurate localization and demonstrate better recovery from broken state estimates. We quantitatively validated such improvements in localization accuracy and recovery using synthetic data with various GPS trajectories and configurations. Experimentally, the constant velocity model with two velocity constraints exhibited around 25% less position error and 70% less orientation error on average compared to the original constant velocity model. We also qualitatively observed similar results with two real-world datasets. In our experiments with real-world datasets, two velocity constraints successfully resolved state ambiguities after abrupt motion and severely incorrect GPS measurements. Our basic implementation is available at https://github.com/mint-lab/filtering_tutorial.

INDEX TERMS GNSS, GPS-only localization, position-only localization, target tracking, EKF localization, state variable ambiguity, velocity constraints.

I. INTRODUCTION

GPS is the most popular sensor for outdoor localization of vehicles, ships, airplanes, drones, bicycles, and smartphones. Its global coverage and accessibility have led to many applications and products. However, GPS systems are not perfect because of their limitation as satellite-based systems using radio signals. GPS signals are sometimes unavailable (e.g. in tunnels and indoors due to signal blockage) and severely inaccurate (e.g. in urban canyons and forests due to multipath propagation). Some researchers have investigated *GPS-less* outdoor localization [1] and developed technologies for coping with partial *GPS outages* [2]. Nevertheless, many researchers and engineers agree that GPS is still practical and useful for outdoor localization and have adopted it for many applications and products.

The associate editor coordinating the review of this manuscript and approving it for publication was Ángel F. García-Fernández .

There have been three research approaches for better *GPS-based* localization, especially for higher accuracy and larger coverage. Firstly, GPS systems have been improved themselves. Differential GPS (D-GPS) and real-time kinematic GPS (RTK-GPS) are well-known enhancements using an extra reference station to correct their received signal to a more accurate pseudo-range. Multi-frequency and multi-constellation GNSS can achieve higher accuracy with more signals from multiple frequency bands and satellites across GPS, GLONASS, BeiDou, and Galileo. Moreover, GPS subsystems (e.g. antennas [3] and signal processing [4], [5], [6], [7]) and algorithms (e.g. trilateration [8], [9], [10], [11]) are also fundamental factors to advance GPS. Secondly, additional sensors have been utilized to compensate for the weakness of GPS. An inertia measurement unit (IMU) has been a popular partner of GPS in aerospace, military, and vehicular applications [2], [12], [13]. A wheel odometer and speedometer are good alternatives for IMUs for wheeled

mobile robots and ground vehicles [14]. A camera [15] and LiDAR [16] are other promising counterparts that provide rich observation of their operating space enough for local and global localization clues. Thirdly, prior information has played a practical role in many real-world applications. For example, a map is useful prior information to restrict GPS position and trajectories to feasible regions or routes. Road maps [13], [17] and appearance data (e.g. images, point clouds, grid/voxels, and meshes) [18] are examples, which are often incorporated with additional sensors and observations.

GPS-only localization is a positioning technique solely using GPS data with no additional sensor and infrastructure. Even though GPS-only localization has apparent limitations in coverage and accuracy due to signal blockage and multipath propagation, it is necessary and important because many products and systems have only GPS for their outdoor positioning. For example, car navigation devices rely solely on GPS for real-time localization and guidance. GPS has been utilized as a single location sensor for geodesic surveying, emergency locators, and asset trackers. Recently, GPS-enabled smartwatches have become popular for runners and bike riders to record their trajectories and activities. Some action cameras or high-end digital cameras have GPS to geotag their photos with the location where they were taken. GPS-only localization is a subset of position-only localization, so its ideas can be extended to broader applications including target (or object) tracking.

This paper proposes two velocity constraints to make GPS-only localization more accurate and resilient (better recovery from its disrupted states). Even though GPS systems are mostly useful in outdoor localization, their position observations can be seriously inaccurate due to multipath propagation. These unreliable observations, so-called *outliers*, make the localization method broken and disrupted. Furthermore, accurate observations can also adversely affect localization algorithms when the GPS trajectories deviate from the assumptions underlying the localization algorithms. For example, abrupt stop and rotation in GPS trajectories violate the constant linear and angular velocity assumption, which can lead to incorrect estimates in the localization algorithms. This paper points out that GPS-only localization fails to recover from such incorrect situations due to its inherent ambiguities of state variables. To resolve the ambiguities, this paper proposed GPS-only localization enhanced by two additional velocity constraints in the framework of Bayesian filtering. Our contributions are more specifically as follows.

- We propose the first constraint, heading angle correction, to fix inverted heading orientation and linear velocity.
- We propose the second constraint, angular rate saturation, to limit angular velocity to prevent it from diverging to a large value.
- We incorporated two constraints to the extended Kalman filter (EKF) localization framework.

- We also share our basic implementation¹ for better clarity and reproducibility of our ideas.

Our two types of experiments with synthetic and real datasets demonstrated the additional constraints achieved better accuracy and recovery, both without and with outliers. In particular, additional constraints were more effective in more noisy and less frequent GPS data, which are common situations for consumer-grade GPS systems.

This paper is organized as follows. At first, Section II reviews related works on GPS-only localization, especially about motion models and tracking with additional constraints. Section III starts with our problem formulation of GPS-only localization and investigates the ambiguities of its state variables. The section also introduces two additional velocity constraints to resolve the ambiguities in GPS-only localization. Section IV contains experimental results with synthetic data generated with the known true trajectories with and without outliers. The ablation study conducted with synthetic data presented the effectiveness of two velocity constraints in improving accuracy. The experiments were further quantitatively validated with various GPS specifications (e.g. GPS observation noise and acquisition frequency) as well as different characteristics of trajectories. Section V presents experimental results with two distinct real datasets: our *DRB Loader* dataset and the *ETRI DeepGuider* dataset [19]. Although quantitative error values cannot be derived due to the absence of ground truth in two real datasets, the qualitative analysis demonstrated that the proposed method had better recovery after falling into state ambiguities. Finally, Section VI ends with a summary and further expected extensions of the proposed method.

II. RELATED WORKS

There have been significant previous works closely related to GPS-only localization and its improvements for better accuracy and resilience. In this section, we review the previous works and highlight our approach compared to them.

A. GPS-ONLY LOCALIZATION

Location estimation using only GPS data is often the first and initial setting adopted by many products and solutions due to its simplicity. As mentioned in Section I, there have been numerous works incorporating additional sensors [12], [14], [15], [16] and prior information [13], [17], [18] to improve GPS-based localization. However, in the absence of additional sensors and prior information, GPS-only localization has been investigated to compensate for its shortcomings.

The first approach pursues improvements in GPS hardware and signal processing. COIN-GPS [3] adopted a directional antenna for indoor coverage and availability. The non-line-of-sight (shortly NLOS) effect was modeled to reduce pseudo-range error in urban canyons [6]. The multipath effect, a well-known challenge in GPS signal processing, has

¹https://github.com/mint-lab/filtering_tutorial

been extensively studied [4], [5]. Recently, random forest regression was utilized to mitigate the multipath effect by filtering out reflected signal components [7].

The second approach aims to enhance localization algorithms using raw GPS data. The factor graph optimization with GPS pseudo-ranges and RTK data (carrier phase and Doppler velocity measurements) was also proposed to improve positioning accuracy [8]. Similarly, relative GPS positions were estimated by the graph optimization additionally with Time-Relative RTK-GNSS factors for loop closure [20]. Learning-based methods have been employed to improve GPS-only localization. Kanhere et al. [9] used the set transformer encoder-decoder architecture with LOS vectors and pseudo-range residual as features. Mohanty and Gao [21] integrated a graph neural network and a learnable Kalman filter with various features such as LOS vectors, pseudo-range residual/uncertainty, and C/N0 values. PrNet [10] proposed a satellite-wise multilayer perceptron to regress pseudorange error using Android raw GNSS measurements. PositionNet [11] trained neural residual maps to cope with urban canyons.

The third approach utilizes only GPS position data (in the form of longitude, latitude, and altitude) available in any GPS system. This approach is considered as *position-only localization*, distinguishing it from range-only and bearing-only localization. Position data can be obtained not only from GPS systems but also from other sensors such as radio beacons, RADAR, and LiDAR. Position-only localization has been extensively studied as a part of (multiple) *target tracking* [22], [23]. Bayesian filtering has been widely employed in position-only localization [22], [23], [24], [25], [26]. As examples of position-only localization with GPS, Aloï and Korniyenko [24] compared the position accuracy of two different filters: a double exponential filter and a Kalman filter. In their evaluation, the two methods demonstrated similar accuracy with their synthetic data, but their modified double exponential filter had significantly better accuracy with their real dataset. In the framework of EKF localization, Choi and Kim [25] revealed that position data from an off-centered GPS could improve position and orientation accuracy mathematically and experimentally. Na et al. [26] further investigated an interacting multiple model (shortly IMM) filter, which incorporates multiple motion models and state representations.

Our Approach: In this paper, we focus on the third approach because raw GPS data are sometimes not available in low-cost GPS systems (e.g. Ascen Korea GPS620 used in the *ETRI DeepGuider* dataset). We aim for position-only localization applicable to all GPS systems from consumer-grade GPS to more advanced GPS. Specifically, we improve the accuracy of position-only localization with Bayesian filtering and two velocity constraints.

B. HANDLING GPS OUTLIERS

Sometimes, GPS data can be substantially corrupted due to its inherent limitation as a radio-based localization system.

When the multipath phenomenon is severe (e.g. in urban canyons), its GPS position becomes highly inaccurate, exhibiting large bias errors. Such inaccurate GPS data can be considered as *outliers*, which may cause degeneration in localization algorithms. There have been many works related to outlier detection and rejection. In conjunction with Bayesian filtering, the Mahalanobis distance has been commonly utilized as a probabilistic distance measure considering the state covariance. For example, Chae et al. [27] rejected highly inaccurate GPS observation using the Mahalanobis distance and predefined thresholds. In nonlinear optimization, robust kernels (also known as robust loss functions) can be employed to mitigate the influence of outliers by assigning lower weights to them. For example, Ch'ng et al. [28] utilized the M-estimator with the Cauchy kernel for their GPS/INS fusion. Fake GPS data generated by GPS spoofing attacks can be considered similar to outliers. To detect the fake GPS data, Zhou et al. [29] exploited the velocity consistency from two different sources: Doppler measurements and pseudo-ranges.

Our Approach: In this paper, we point out that GPS-only localization can fall into degeneracy (or ambiguity) not only due to outliers but also due to normal data as demonstrated in Section IV. We do not tackle outlier detection and rejection as explored in the above previous works. Instead, we aim to enhance the resilience of GPS-only localization with two velocity constraints by recovering from degenerated (or ambiguous) states.

C. CONSTRAINTS FOR MOTION MODELS AND BAYESIAN FILTERING

A constraint can be useful in solving a problem because it restricts the solution space. That's why a constraint is sometimes referred to as *prior knowledge*.

A motion model describes how a target object is expected to move over time and may contain specific kinematic or dynamic constraints that are beneficial for target tracking and localization. Na et al. [26] explored four combinations of different motion constraints (constant speed and constant turn rate) and their representations in two coordinate systems (polar and Cartesian coordinates) for target tracking. They showed that their four combinations exhibited varying performances in different trajectories according to their constraints. They incorporated the four combinations into an IMM filter and demonstrated the best accuracy in various synthetic and real datasets. Westny et al. [30] examined a range of motion models (from pure integrators to kinematic models and neural ODEs) for trajectory prediction using their graph neural networks. They found that a simple constant velocity model (denoted as 1XI in their notation) yielded the best result in the public highway and roundabout datasets. Choi et al. [31] improved heading estimation using the average of two velocities derived by GPS and INS, respectively.

Bayesian filtering can be incorporated with a constraint. The smooth variable structure filter (shortly SVSF) [32]

is a novel filtering technique based on the Kalman filter and sliding mode concept. The SVSF can yield smoother estimates within its smoothing boundary layer by applying a saturation function to innovation residuals of observations. The SVSF has been applied to numerous applications and enhanced through various variants. Li et al. [33] proposed Tanh-SVSF, utilizing the hyperbolic tangent function as a new saturation function for better chattering suppression. They applied their Tanh-SVSF to the target tracking under model uncertainty and presented better accuracy than the original SVSF. Akhtar et al. [34] combined multiple filters (EKF, unscented Kalman filter (UKF), cubature Kalman filters (CKF), and SVSFs) and achieved better accuracy in target tracking.

Our Approach: In this paper, we propose two velocity constraints based on prior knowledge of motion patterns. Our angular rate constraint is implemented using the hyperbolic tangent function, which is similar to the Tanh-SVSF but its utilization is quite different. The Tanh-SVSF uses the hyperbolic tangent function to saturate the innovation residuals, but we utilize it to saturate angular velocity.

III. GPS-ONLY LOCALIZATION WITH TWO VELOCITY CONSTRAINTS

A. PROBLEM FORMULATION

GPS-only localization estimates the position and orientation of a target object only with position observation from GPS. For simplicity, we assume that the target object is a vehicle on a two-dimensional plane. The position and orientation of the vehicle on a 2D plane are represented as (x, y) and θ . The linear and angular velocity of the vehicle are described as v and w , respectively. GPS provides a 2D position observation written as (x^g, y^g) .

GPS-only localization determines the vehicle pose (x, y, θ) solely based on GPS observation (x^g, y^g) . Some approaches incorporate kinematic (or dynamic) motion models, so they can additionally estimate the vehicle velocity (v, w) (or more). The dimension of unknown variables is 3 to 5 (including velocity) but the dimension of GPS observation is just 2. Therefore, GPS-only localization can suffer from ambiguities among unknown variables if there are no appropriate models and constraints. In our experience, well-initialized GPS-only localization also struggles with such ambiguities when motion or observation assumptions are violated (e.g. severely inaccurate GPS measurements).

B. EKF LOCALIZATION

In this paper, our GPS-only localization is based on the extended Kalman filter (EKF), one of the most popular Bayesian filtering in localization. Even though this paper is completely based on EKF, the proposed ideas can be applied to other techniques of Bayesian filtering. EKF is a nonlinear extension of the Kalman filter. EKF is iterations of state prediction (with a motion model) and correction (with an observation model) steps. The two steps are mathematically described in Algorithm 1. In our EKF localization, the state

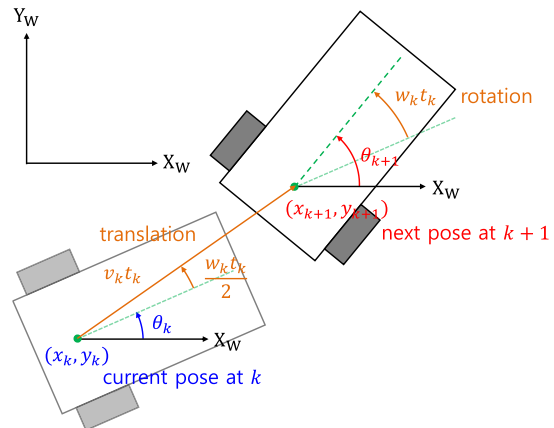


FIGURE 1. Constant velocity (CV) motion model: The next pose is derived from the current pose and translational and rotational displacements. (X_W and Y_W axes are the world coordinate.)

variable is defined as $\mathbf{x}_k = [x_k, y_k, \theta_k, v_k, w_k]^T$ where k means the k -th timestamp. Our EKF localization was built upon our previous work [25] with the constant velocity (CV) motion model and off-centered GPS observation model.

CV Motion Model: The CV model assumes zero linear and angular acceleration, resulting in constant linear and angular velocity. Since the constant linear and angular velocity implies an unchanged turning radius (curvature), the CV model is also referred to as the constant turn rate and velocity (CTRV) model. The CV model predicts its next state \mathbf{x}_{k+1} using the current velocity and time elapsed after the last state update. As depicted in Figure 1, the CV model accumulates translational and rotational displacements while maintaining constant linear and angular velocity as

$$\mathbf{x}_{k+1} = f^{CV}(\mathbf{x}_k; t_k) = \begin{bmatrix} x_k + v_k t_k \cos(\theta_k + \frac{w_k t_k}{2}) \\ y_k + v_k t_k \sin(\theta_k + \frac{w_k t_k}{2}) \\ \theta_k + w_k t_k \\ v_k \\ w_k \end{bmatrix}, \quad (1)$$

where t_k is the time interval $(T_{k+1} - T_k)$ between the time at the last state update (T_k) and the time at the next state update (T_{k+1}) .

Off-Centered GPS Model: The off-centered GPS [25] is a more generalized GPS observation model that considers the placement of a GPS antenna on the vehicle. As shown in Figure 2, the location of GPS is specified by its installation offset (o_ρ, o_ϕ) from the center of the vehicle. It is common to define the vehicle center and local coordinate (X_V, Y_V) at the middle of the rear wheels because the wheels do not move laterally. The advantage of off-centered GPS for better localization accuracy has been theoretically and experimentally verified [25]. GPS provides the position observation $\mathbf{z}_k = [x_k^g, y_k^g]^T$ and the off-centered GPS model incorporates the installation offset as

$$\mathbf{z}_k = h(\mathbf{x}_k) = \begin{bmatrix} x_k + o_\rho \cos(\theta_k + o_\phi) \\ y_k + o_\rho \sin(\theta_k + o_\phi) \end{bmatrix}. \quad (2)$$

The Jacobian matrix of the off-centered GPS model is derived as

$$H_k = \frac{\partial}{\partial \mathbf{x}_k} h(\mathbf{x}_k) = \begin{bmatrix} 1 & 0 & -o_\rho \sin(\theta_k + o_\phi) & 0 & 0 \\ 0 & 1 & o_\rho \cos(\theta_k + o_\phi) & 0 & 0 \end{bmatrix}, \quad (3)$$

The centered GPS is a special case of Equation (2) with zero offset, $o_\rho = 0$.

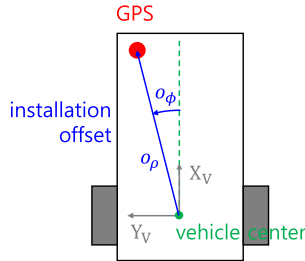


FIGURE 2. Off-centered GPS observation model: GPS is installed at the radial and angular offsets (o_ρ, o_ϕ) from the center of the vehicle. (X_V and Y_V axes are the local coordinate attached to the center of the vehicle.)

C. STATE AMBIGUITIES IN GPS-ONLY LOCALIZATION

GPS-only localization can utilize only position measurements, so it inherently suffers from ambiguities in its state variables. These ambiguities arise from unobserved state variables and their mutual entanglements. Even though GPS-only localization initializes with the good state variables, it frequently becomes trapped in these ambiguities and is not recovered. Highly noisy GPS measurements (so-called as *outliers*) are a representative example of contaminating the state variables. The degenerated state variables are not recovered even though GPS measurements return to normal with small noise. From our observation, the state variables can fall into the ambiguities without outliers when a vehicle undergoes abrupt movements (e.g. urgent heading change and sudden stop). This is because such abrupt movements result in significant changes in linear and angular velocity, thereby violating the above assumption of the CV model (zero acceleration).

The first ambiguity is the *unknown directions of vehicle heading and linear velocity*. As shown in Figures 3a and 3b, the positive linear velocity with forward orientation produces the same position observations as the negative linear velocity with inverted heading orientation. Only from a series of position observations, it is impossible to distinguish between moving forward (θ, v) and moving backward ($\theta + \pi, -v$). One of the fundamental solutions is heading angle estimation with dual GPS antennas. However, this approach needs additional hardware and sufficiently good GPS accuracy beyond the baseline between two GPS antennas. There are some commercial GPS receivers to deal with two antennas together, which are mostly based on RTK-GPS or D-GPS systems to distinguish the heading direction.

The second ambiguity is the *unknown scale of linear and angular velocity*. As shown in Figure 3c, amplified linear and angular velocity can satisfy the curvature of GPS

trajectories (e.g. $\kappa = w/v = 2w/2v = \dots$; κ : curvature). The amplified angular velocity can also fulfill the moving direction condition such as $w + 2\pi n$ (n : integer multiplier). In addition, as depicted in Figure 3d, the state variables can exhibit extra spinning motion when the angular velocity is extremely increased, $w \gg 0$, while the linear velocity remains similar to v . Since the angular velocity is typically small but prone to be incorrectly amplified, the constant steering and velocity (CSAV) motion model has been employed to overcome such ambiguity and divergence of angular velocity.

CSAV Motion Model: The CSAV model incorporates an assumption of zero angular velocity in addition to the CV model. Since its angular velocity is always zero, the CSAV model has zero rotational displacement, thus its transition function maintains the heading angle constant, $\theta_{k+1} = \theta_k$. The state variables of the CSAV model are generally defined without the angular velocity because it is always zero. Therefore, with the simplified state variable $\mathbf{x}_k = [x_k, y_k, \theta_k, v_k]^T$, the CSAV model predicts its subsequent state as

$$\mathbf{x}_{k+1} = f^{CSAV}(\mathbf{x}_k; t_k) = \begin{bmatrix} x_k + v_k t_k \cos(\theta_k) \\ y_k + v_k t_k \sin(\theta_k) \\ \theta_k \\ v_k \end{bmatrix}. \quad (4)$$

The CSAV model is a special case of the CV model with the additional constraint, $w_k = 0$, which can relieve the second ambiguity derived by amplified angular velocity. This additional constraint is usually reasonable because straight motion (or large-curvature motion) is the most common in many navigation situations. Even though there is no update in the heading orientation θ_k , it is gradually updated toward appropriate values due to the noise terms in Bayesian filtering. Therefore, it is typical for the CSAV model to assign a larger covariance to the state transition noise than the CV model. As shown in Figure 7, the CSAV model exhibited the highest accuracy when using a larger value for the rotational noise parameter.

However, the CSAV model performs poorly in highly rotational motion patterns because it assumes zero angular velocity. This limitation becomes evident, for example, with a small turning radius (e.g. during in-place rotation of a differential drive). In such scenarios, where the vehicle undergoes significant rotation motion, the CSAV model fails to accurately track orientation changes, resulting in delayed position estimates.

D. PROPOSED GPS-ONLY LOCALIZATION WITH TWO VELOCITY CONSTRAINTS

In this paper, we propose two different velocity constraints to overcome the ambiguities inherent in position-only localization. Two velocity constraints are incorporated with our previous EKF localization [25]. However, we believe

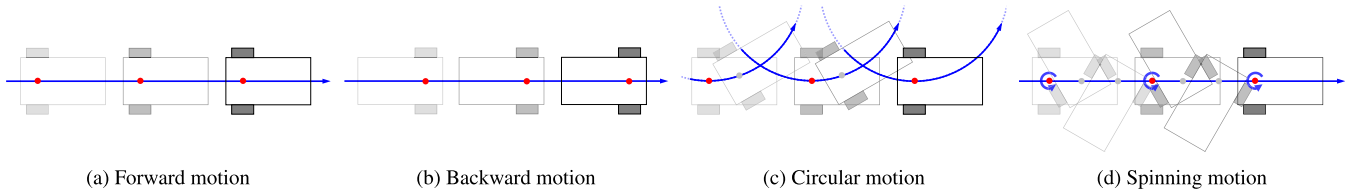


FIGURE 3. Examples of state ambiguities due to confusion of unobserved state variables: The same GPS observations (red dots) can be observed from four different sets of trajectories (blue lines) and state variables. For simplicity, the GPS is located at the center of the vehicle.

these constraints can be applied to not only EKF but also other Bayesian filtering such as UKF and particle filters.

1) HEADING ANGLE CORRECTION

The first constraint, heading angle correction, aims to resolve the first ambiguity of heading angle and linear velocity. This constraint stems from an additional prior, the known moving direction of a vehicle. Typically, vehicles move forward except in rare scenarios. Given the assumption that the vehicle always moves forward ($v_k \geq 0$), we can apply the constraint as follows:

$$\mathbf{x}_k = \begin{cases} [\bar{x}_k, \bar{y}_k, \theta_k + \pi, -v_k, w_k]^\top & \text{if } v_k < \epsilon_- \\ \mathbf{x}_k & \text{otherwise} \end{cases}, \quad (5)$$

where (\bar{x}_k, \bar{y}_k) is the inverse of the vehicle position concerning the off-centered GPS as

$$\bar{x}_k = x_k + 2 o_\rho \cos(\theta_k + o_\phi) \quad (6)$$

$$\bar{y}_k = y_k + 2 o_\rho \sin(\theta_k + o_\phi) \quad (7)$$

and ϵ_- is the linear velocity threshold of backward motion. In our experiments, we defined the threshold ϵ_- as a small negative number, -0.001 m/s. In the case of $\epsilon_- = 0$, undesired frequent heading switching had been observed particularly at extremely slow speed. The reason why we used a small negative number (not zero) is similar to the reason why we use hysteresis thresholding against noise. In contrast, when the threshold has a large value ($\epsilon_- \gg 0$), it is similar to operating *without* the heading angle correction because the correction is rarely activated. Our experiments shown in Figure 8 also support our discussion on the backward motion threshold ϵ_- . As presented in Algorithm 1, the heading angle correction is implemented as a post-processing after the state correction step.

The heading angle correction can be extended for more general cases. For instance, if the vehicle is moving backward, the heading switching condition can be modified to $v_k > \epsilon_+$, where ϵ_+ is the velocity threshold of forward motion (a small positive value). Sometimes a vehicle needs to move forward and also backward. If its moving direction is available or known (e.g. via navigation commands or transmission shifters), the heading switching condition can be extended as

$$(d_k \text{ is } F \text{ and } v_k < \epsilon_-) \text{ or } (d_k \text{ is } B \text{ and } v_k > \epsilon_+), \quad (8)$$

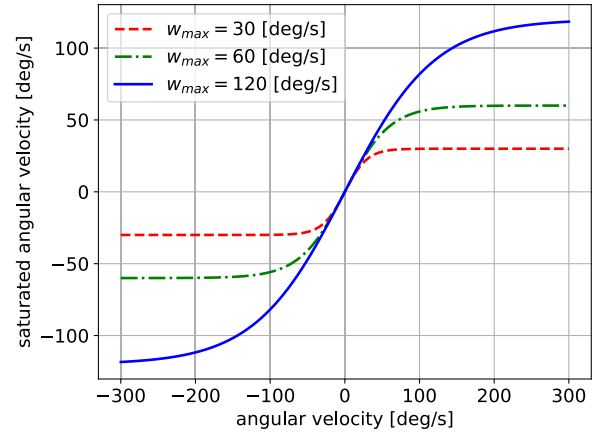


FIGURE 4. Hyperbolic tangent functions with various maximum angular velocities w_{max} .

where d_k is the known moving direction, denoted as forward (as F) or backward (as B).

2) ANGULAR RATE SATURATION

The second constraint, angular rate saturation, can suppress the second ambiguity of amplified angular velocity. This constraint restricts the range of angular velocity using the hyperbolic tangent function as follows:

$$\bar{w}_k = w_{max} \tanh\left(\frac{w_k}{w_{max}}\right), \quad (9)$$

where w_{max} is the maximal value of angular velocity. The maximal angular velocity is sometimes known in advance according to the vehicle specifications or the navigation constraints. In our EKF localization, as shown in Algorithm 1, this constraint is integrated into the EKF prediction step as a modified state transition function. The CV motion model with the angular rate saturation is written as

$$\mathbf{x}_{k+1} = f^{CV+A}(\mathbf{x}_k) = \begin{bmatrix} x_k + v_k t_k \cos(\theta_k + \frac{w_k t_k}{2}) \\ y_k + v_k t_k \sin(\theta_k + \frac{w_k t_k}{2}) \\ \theta_k + w_k t_k \\ v_k \\ w_{max} \tanh(w_k / w_{max}) \end{bmatrix}. \quad (10)$$

To confine the range of angular velocity, we adopt the hyperbolic tangent function because it is smooth and differentiable as shown in Figure 4. Thanks to its properties,

the Jacobian matrix of Equation (10) is derived as

$$F_k^{CV+A} = \frac{\partial}{\partial \mathbf{x}_k} f^{CV+A}(\mathbf{x}_k; t_k) = \begin{bmatrix} 1 & 0 & -v_k t_k s_k & t_k c_k & -v_k t_k^2 s_k / 2 \\ 0 & 1 & v_k t_k c_k & t_k s_k & v_k t_k^2 c_k / 2 \\ 0 & 0 & 1 & 0 & t_k \\ 0 & 0 & 0 & 1 & 0 \\ 0 & 0 & 0 & 0 & 1 - \bar{w}_k^2 \end{bmatrix}, \quad (11)$$

where s_k and c_k are short notations for $\sin \theta_k$ and $\cos \theta_k$, respectively.

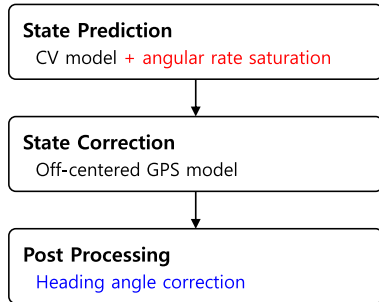


FIGURE 5. Bayesian GPS-only localization with two velocity constraints: Two colored parts are added to the original GPS-only localization [25].

3) OVERALL LOCALIZATION PROCEDURE

GPS-only localization with two velocity constraints is briefly described in Figure 5 and Algorithm 1. The angular rate saturation is applied in the state prediction. The heading angle correction is performed after the state correction if its switching condition is satisfied. In the framework of EKF, it estimates the current state variables \mathbf{x}_k and its covariance P_k from the previous state variables \mathbf{x}_{k-1} , covariance P_{k-1} , and current GPS observation \mathbf{z}_k . The matrix Q_{k-1} is the covariance matrix of the state transition noise. Since a vehicle generally exhibits translational and rotational motion uncertainty [35], we derived the covariance Q_{k-1} as

$$Q_{k-1} = W_{k-1} \begin{bmatrix} \sigma_v^2 & 0 \\ 0 & \sigma_w^2 \end{bmatrix} W_{k-1}^T, \quad (12)$$

where σ_v^2 and σ_w^2 are the variance of noises related to linear and angular velocity, respectively. The matrix W_{k-1} is the Jacobian matrix of Equation (10) with respect to the velocity $\mathbf{v}_{k-1} = [v_{k-1}, w_{k-1}]^T$ as follows:

$$W_{k-1} = \frac{\partial}{\partial \mathbf{v}_{k-1}} f^{CV+A}(\mathbf{x}_k; t_k) = \begin{bmatrix} t_{k-1} c_{k-1} & -v_{k-1} t_{k-1}^2 s_{k-1} / 2 \\ t_{k-1} s_{k-1} & v_{k-1} t_{k-1}^2 c_{k-1} / 2 \\ 0 & t_{k-1} \\ 1 & 0 \\ 0 & 1 - \bar{w}_{k-1}^2 \end{bmatrix}. \quad (13)$$

The matrix R_k is the covariance matrix of the state observation noise as

$$R_k = \begin{bmatrix} \sigma_G^2 & 0 \\ 0 & \sigma_G^2 \end{bmatrix}, \quad (14)$$

where σ_G^2 is the variance of GPS noises. The function `TrimRadian` converts the given angle within $[-\pi, \pi)$.

Algorithm 1 EKF-Based GPS-Only Localization With Two Velocity Constraints

Input: $\mathbf{x}_{k-1}, P_{k-1}, t_{k-1}, \mathbf{z}_k$

Output: \mathbf{x}_k, P_k

begin

// State prediction with angular rate saturation

$\hat{\mathbf{x}}_k \leftarrow f^{CV+A}(\mathbf{x}_{k-1}; t_{k-1})$

$\hat{P}_k \leftarrow F_{k-1}^{CV+A} P_{k-1} F_{k-1}^{CV+A \top} + Q_{k-1}$

// State correction

$\mathbf{x}_k \leftarrow \hat{\mathbf{x}}_k + K_k (\mathbf{z}_k - h(\hat{\mathbf{x}}_k))$

$K_k = \hat{P}_k H_k^T (H_k \hat{P}_k H_k^T + R_k)^{-1}$

$P_k = (I - K_k H_k) \hat{P}_k$

// Heading angle correction

if $v_k < \epsilon_-$ **then**

$x_k \leftarrow x_k + 2 o_\rho \cos(\theta_k + o_\phi)$

$y_k \leftarrow y_k + 2 o_\rho \sin(\theta_k + o_\phi)$

$\theta_k \leftarrow \text{TrimRadian}(\theta_k + \pi)$

$v_k \leftarrow -v_k$

end

end

IV. EXPERIMENTS WITH SYNTHETIC DATA

Synthetic GPS data were used to analyze various characteristics of the proposed GPS-only localization with two velocity constraints. Since the synthetic data were generated based on predefined true poses and velocities of a simulated vehicle, we could easily evaluate experimental results compared to the known ground truth. Moreover, we could specify the simulated GPS (e.g. acquisition frequency and installed location) and control its observation situations (e.g. GPS noise and outliers) as we wanted.

A. CONFIGURATION

1) TRAJECTORIES

Four different types of trajectories were utilized to generate the synthetic GPS data. Figure 6 presents four vehicle trajectories whose traversal distances are around 100 meters, respectively. *Straight line* trajectory is simple, but it reflects the most common navigation scenario, moving forward with constant linear velocity and zero angular velocity. *Circle* trajectory is considered for constant angular velocity, and *sine wave* trajectory contains varying angular velocity with smooth curvature changes. *Square wave* trajectory contains abrupt heading changes, which can sometimes trigger the state ambiguities only with small GPS noise.

2) GPS DATA GENERATION

GPS measurements were generated from the virtual GPS installed on a virtual vehicle. We can control its placement

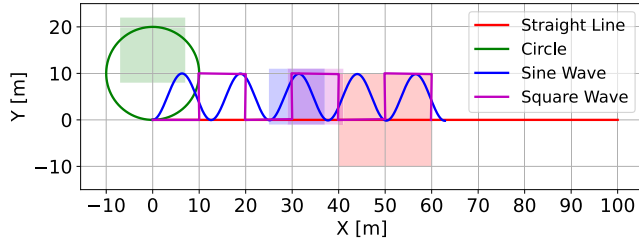


FIGURE 6. Four types of trajectories and their corresponding dead zones (as same colored boxes).

on the vehicle, and its off-centered measurements can be simulated by Equation (2). We installed the virtual GPS at $o_\rho = 1$ meter for the off-centered GPS setting and $o_\rho = 0$ for the centered GPS setting. In both settings, there was no angular offset, $o_\phi = 0$. We applied the unbiased Gaussian noise to the GPS measurements as

$$x_k^G = x_k^* + o_\rho \cos(\theta_k^* + o_\phi) + \mathcal{N}(0, \sigma_G^2) \quad (15)$$

$$y_k^G = y_k^* + o_\rho \sin(\theta_k^* + o_\phi) + \mathcal{N}(0, \sigma_G^2), \quad (16)$$

where $(x_k^*, y_k^*, \theta_k^*)$ is the true position and orientation of the vehicle at k -th timestamp, and $\mathcal{N}(0, \sigma_G^2)$ is a random number generated by the Gaussian distribution with zero mean and σ_G^2 variance. In the default configuration, we set GPS noise to $\sigma_G = 0.5$ meters and GPS acquisition frequency to 1 Hz. The default value of σ_G was derived from a recent U.S. FAA report [36], which stated that their high-quality and single-frequency GPS receivers had the horizontal position error bound of 1.82 meters ($3\sigma_G \approx 1.82$). The default value of GPS acquisition frequency was chosen as 1 Hz because it is the most common in many GPS receivers. However, as shown in Figures 13 and 14, we also varied the GPS noise and acquisition frequency to analyze their effect on our proposed velocity constraints.

Similarly, outliers (severely inaccurate GPS measurements) were generated by the unbiased Gaussian distribution with a significantly larger variance. Based on our experience with GPS, outliers were observed as a series of seriously noisy data due to its surrounding structures (e.g. tall buildings). We generated outliers with higher GPS noise as much as $\sigma_G = 10$ meters that was derived from the rough law of urban multipath [37] in the case of 5-floor buildings. In addition, outliers were not sporadic but rather occurred as a long series within specific areas. We defined a rectangular dead zone on each trajectory, and outliers were generated within the dead zone. Figure 6 also highlights each dead zone, and Figure 12 presents an example trajectory with outliers. Based on our outlier setting, each trajectory contained approximately 20% – 25% outliers.

3) ALGORITHM PARAMETERS

The performance of EKF-based localization depends on its configuration parameters, which were selected as their optimal values to be the most accurate. For the state transition noise, we found the optimal set of motion noises using a grid search. Figure 7 illustrates a snapshot of our grid search with

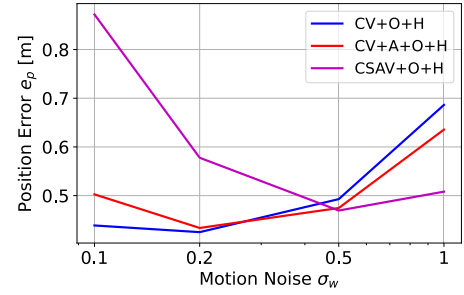


FIGURE 7. Position error e_p with varying motion noise σ_w on all types of trajectories.

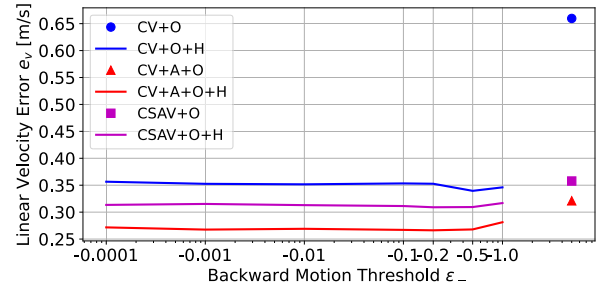


FIGURE 8. Linear velocity error e_v with varying backward motion threshold ϵ_- on all types of trajectories.

a logarithmic variation of parameters. We set $\sigma_v = \sigma_w = 0.2$ for the CV model and its variants, and $\sigma_v = \sigma_w = 0.5$ for the CSAV model and its variants. For the state observation noise, the optimal value of GPS noise σ_G was already known because we generated the GPS data.

Two velocity constraints also contain some parameters, which were set to their optimal values. For the heading angle correction, we found the optimal value of the backward motion threshold ϵ_- us. Figure 8 presents our grid search with a logarithmic variation of parameters. It shows that the sensitivity of the backward motion threshold was quite moderate in the large range of values $[-0.5, -0.0001]$. We set ϵ_- to -0.001 m/s in our experiments. For the angular rate saturation, we set the maximum angular velocity w_{max} as 1 rad/s (around 57.2 deg/s) because abrupt rotation (high angular velocity) is quite rare in typical navigation scenarios.

4) EVALUATION CRITERIA

Localization accuracy is simply quantified using the true position and orientation of the vehicle. Position, orientation, and velocity errors of the estimated vehicle trajectory are calculated as follows:

$$e_p = \text{median} \{ (x_k^* - x_k)^2 + (y_k^* - y_k)^2 \mid \forall k \} \quad (17)$$

$$e_o = \text{median} \{ |\text{TrimRadian}(\theta_k^* - \theta_k)| \mid \forall k \} \quad (18)$$

$$e_v = \text{median} \{ |v_k^* - v_k| \mid \forall k \} \quad (19)$$

$$e_w = \text{median} \{ |w_k^* - w_k| \mid \forall k \}, \quad (20)$$

where median returns the median value of given series of errors. We adopted the median as a representative value for each trajectory because it provides a more robust measure than averaging in the presence of outliers. For statistically

TABLE 1. Configuration of ablation study: In state variables, V, C, and 0 represent varying, constant, and zero values in motion models, respectively. S means a saturated variable with the hyperbolic tangent function.

| Abbreviation | Motion Models | State Variables | | | | | Off-centered GPS | Heading Angle Correction | Angular Rate Saturation | |
|--------------|---|-----------------|-----|----------|-----|-----|------------------|--------------------------|-------------------------|---|
| | | x | y | θ | v | w | | | | |
| CV | Constant Velocity Equation (1) | | | | | | | | | |
| CV+O | | V | V | V | C | C | v | | | |
| CV+O+H | | | | | | | | v | v | |
| CV+A | CV + Angular Rate Saturation Equation (10) | | | | | | | | v | |
| CV+A+O | | V | V | V | C | S | v | | v | |
| CV+A+O+H | | | | | | | | v | v | v |
| CSAV | Constant Steering And Velocity Equation (4) | | | | | | | | | |
| CSAV+O | | V | V | C | C | 0 | v | | | |
| CSAV+O+H | | | | | | | | v | v | |

TABLE 2. Localization and velocity estimation errors on each type of trajectories with GPS data ($\sigma_G = 0.5$ [m] and 1 Hz) without outliers (units: e_p [m], e_o [deg], e_v [m/s], and e_w [deg/s]): Lower values are better. The cells of the top and second-best values are highlighted in blue and light blue, respectively.

| Methods | Straight Line | | | | Circle | | | | Sine Wave | | | | Square Wave | | | |
|----------|---------------|-------|-------|-------|--------|-------|-------|-------|-----------|-------|-------|-------|-------------|-------|-------|-------|
| | e_p | e_o | e_v | e_w | e_p | e_o | e_v | e_w | e_p | e_o | e_v | e_w | e_p | e_o | e_v | e_w |
| Raw GPS | 0.591 | - | - | - | 0.585 | - | - | - | 0.589 | - | - | - | 0.588 | - | - | - |
| CV | 0.473 | 13.9 | 0.125 | 5.4 | 0.471 | 14.7 | 0.131 | 5.7 | 0.593 | 35.6 | 0.409 | 14.6 | 0.649 | 75.0 | 0.698 | 12.4 |
| CV+O | 0.377 | 8.9 | 0.109 | 4.9 | 0.393 | 9.1 | 0.110 | 5.0 | 0.445 | 11.6 | 0.272 | 9.5 | 0.481 | 12.9 | 0.254 | 8.6 |
| CV+O+H | 0.390 | 9.2 | 0.110 | 4.8 | 0.372 | 9.0 | 0.112 | 4.9 | 0.436 | 11.3 | 0.265 | 9.6 | 0.500 | 13.8 | 0.279 | 8.8 |
| CV+A | 0.473 | 13.6 | 0.122 | 5.1 | 0.472 | 14.2 | 0.128 | 5.4 | 0.572 | 26.1 | 0.305 | 14.3 | 0.626 | 79.2 | 0.733 | 11.2 |
| CV+A+O | 0.378 | 8.9 | 0.109 | 4.8 | 0.392 | 9.1 | 0.109 | 4.7 | 0.442 | 11.5 | 0.271 | 9.2 | 0.474 | 12.8 | 0.250 | 8.6 |
| CV+A+O+H | 0.390 | 9.1 | 0.110 | 4.7 | 0.372 | 8.8 | 0.111 | 4.7 | 0.434 | 11.2 | 0.262 | 9.5 | 0.492 | 13.6 | 0.278 | 8.8 |
| CSAV | 0.492 | 11.0 | 0.195 | - | 0.492 | 11.9 | 0.196 | - | 0.553 | 23.5 | 0.299 | - | 0.563 | 73.5 | 0.624 | - |
| CSAV+O | 0.410 | 9.7 | 0.193 | - | 0.415 | 9.7 | 0.192 | - | 0.446 | 12.4 | 0.241 | - | 0.470 | 13.1 | 0.279 | - |
| CSAV+O+H | 0.419 | 9.5 | 0.200 | - | 0.417 | 9.5 | 0.200 | - | 0.469 | 13.4 | 0.251 | - | 0.539 | 16.1 | 0.307 | - |

TABLE 3. Localization and velocity estimation errors on each type of trajectories with GPS data ($\sigma_G = 0.5$ [m] and 1 Hz) with outliers: Lower values are better. The cells of significantly inaccurate values ($e_o > 50$ [deg], $e_v > 1$ [m/s], and $e_w > 100$ [deg/s]) are highlighted in red.

| Methods | Straight Line | | | | Circle | | | | Sine Wave | | | | Square Wave | | | |
|----------|---------------|-------|-------|-------|--------|-------|-------|-------|-----------|-------|-------|-------|-------------|-------|-------|-------|
| | e_p | e_o | e_v | e_w | e_p | e_o | e_v | e_w | e_p | e_o | e_v | e_w | e_p | e_o | e_v | e_w |
| Raw GPS | 0.700 | - | - | - | 0.716 | - | - | - | 0.680 | - | - | - | 0.785 | - | - | - |
| CV | 0.680 | 40.2 | 0.563 | 154.7 | 0.792 | 44.1 | 0.646 | 137.9 | 0.781 | 68.2 | 1.056 | 194.7 | 0.954 | 73.7 | 0.896 | 181.8 |
| CV+O | 0.549 | 14.4 | 0.295 | 220.0 | 0.666 | 17.4 | 0.754 | 202.4 | 0.593 | 16.3 | 0.750 | 256.1 | 0.720 | 21.2 | 0.615 | 162.3 |
| CV+O+H | 0.587 | 14.7 | 0.199 | 162.9 | 0.774 | 22.0 | 0.296 | 160.1 | 0.627 | 17.8 | 0.354 | 204.5 | 0.828 | 25.4 | 0.493 | 203.1 |
| CV+A | 0.592 | 55.1 | 1.152 | 7.5 | 0.663 | 54.4 | 1.180 | 8.1 | 0.691 | 68.0 | 0.986 | 17.0 | 0.878 | 72.5 | 0.880 | 17.2 |
| CV+A+O | 0.511 | 13.0 | 0.172 | 7.1 | 0.586 | 15.6 | 0.220 | 8.7 | 0.578 | 15.4 | 0.351 | 12.2 | 0.694 | 20.0 | 0.494 | 14.6 |
| CV+A+O+H | 0.485 | 12.1 | 0.156 | 7.0 | 0.541 | 14.6 | 0.189 | 8.1 | 0.540 | 14.9 | 0.314 | 12.1 | 0.711 | 21.3 | 0.460 | 14.2 |
| CSAV | 0.603 | 74.2 | 1.546 | - | 0.636 | 54.5 | 1.463 | - | 0.661 | 36.2 | 0.520 | - | 0.758 | 77.3 | 1.022 | - |
| CSAV+O | 0.536 | 13.8 | 0.285 | - | 0.627 | 16.3 | 0.364 | - | 0.569 | 16.6 | 0.340 | - | 0.662 | 20.3 | 0.461 | - |
| CSAV+O+H | 0.507 | 12.8 | 0.266 | - | 0.564 | 14.9 | 0.287 | - | 0.567 | 17.0 | 0.324 | - | 0.765 | 24.5 | 0.447 | - |

meaningful results, I repeated each experiment configuration 100 times and selected their median as a representative value for the configuration.

B. RESULTS AND DISCUSSION

We analyzed various characteristics of the proposed velocity constraints from different perspectives.

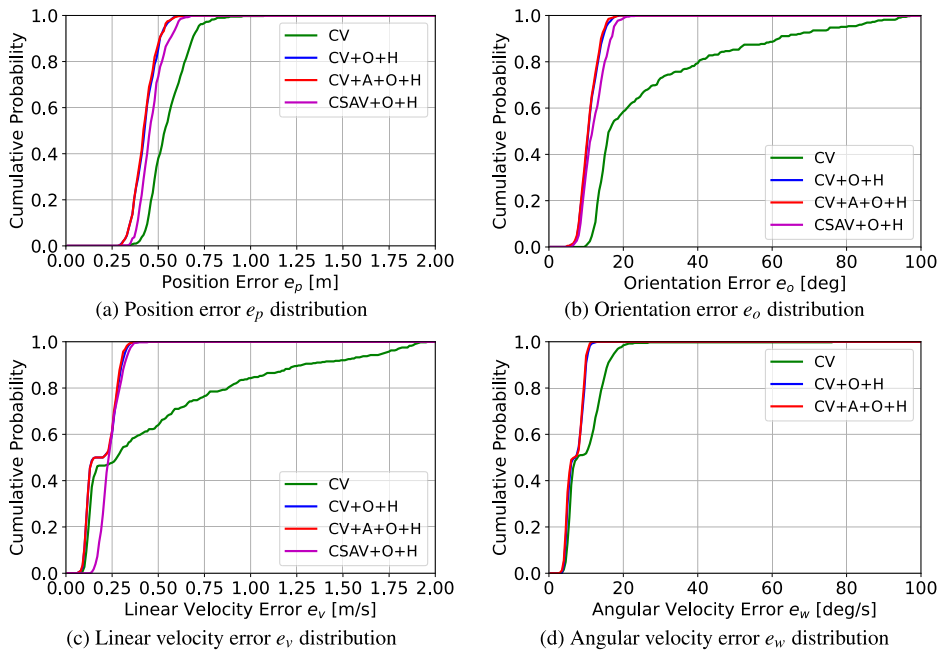


FIGURE 9. Cumulative distribution functions (CDF) of each error measure on all types of trajectories with GPS data ($\sigma_G = 0.5$ meters and 1 Hz) without outliers: The CDF values represent the probability of being less than the given error value on the X-axis. For example, $y = P(e_p \leq x)$ for position error.

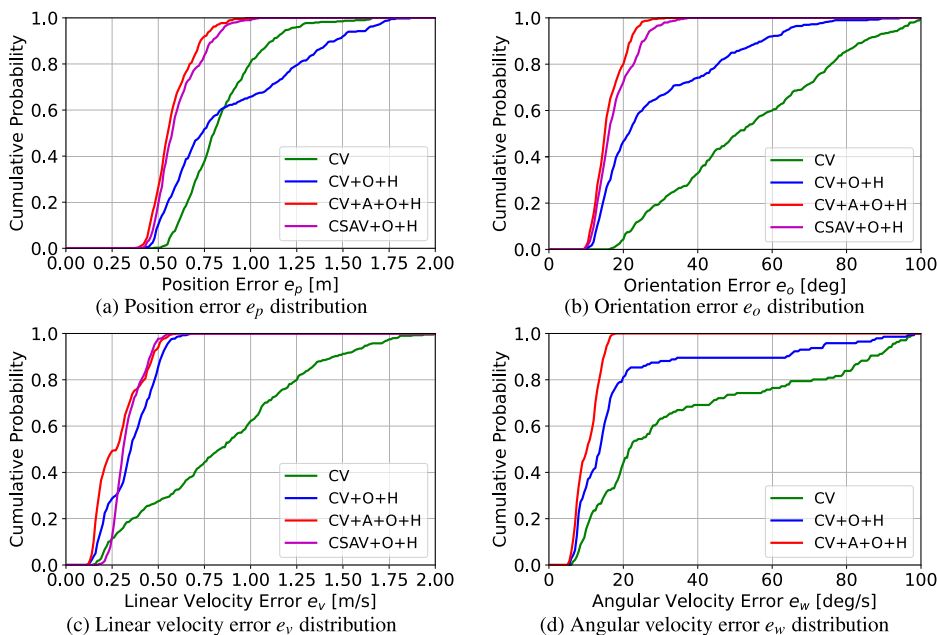


FIGURE 10. Cumulative distribution functions (CDF) of each error measure on all types of trajectories with GPS data ($\sigma_G = 0.5$ meters and 1 Hz) with outliers.

1) ABLATION STUDY

We investigated localization improvement by each velocity constraint *without* and *with* outliers, respectively. Nine combinations of localization methods are presented in Table 1. We applied the off-centered GPS observation ($\rho = 1$) and the heading angle correction to three different motion models including the CV model with the angular rate saturation.

Discussion Without Outliers: Localization and velocity estimation errors *without* outliers and their example

trajectories are presented in Table 2 and Figure 9. Specifically, Figure 9 visualizes cumulative distribution functions of each error measure to compensate for invisible points of median values. Figure 11 also shows a localization example on the *sine wave* trajectory. We could catch the following observations.

Firstly, the proposed methods (CV+A+O and CV+A+O+H) had the best and the second-best results. CV+A+O+H had 23%, 69%, 44%, and 27% less errors than the original CV

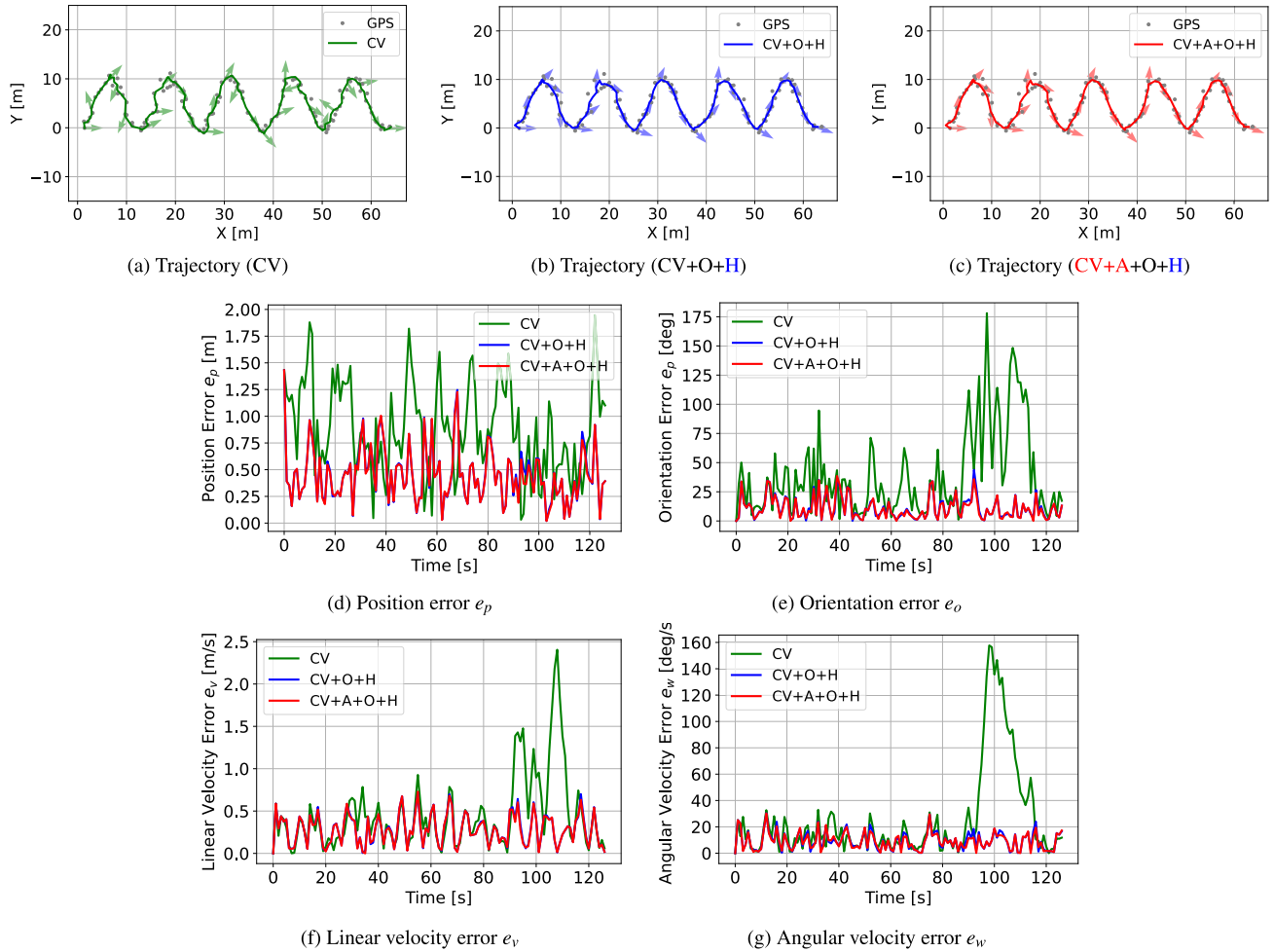


FIGURE 11. Localization and velocity estimation results on the *sine wave* trajectory with GPS data ($\sigma_G = 0.5$ meters and 1 Hz) *without* outliers: The vehicle orientations are represented as arrows at every 5 seconds.

model on average across all trajectories. However, the CV model only with the off-centered GPS observation (CV+O) also achieved good results as the third-best. Localization errors of the three methods were almost similar, and the best method (CV+A+O) was slightly better than the other two methods.

Secondly, the off-centered GPS observation model (+O) improved localization significantly. Especially, its improvements were quite apparent in cases of more varying vehicle orientation and angular velocity such as *sine wave* and *square wave* trajectories. Orientation errors were almost 3 times and 6 times better in *sine wave* and *square wave* trajectories, respectively. As we already discussed in our previous work [25], since the off-centered GPS model reduced uncertainty in vehicle orientation, it could sequentially achieve higher accuracy in vehicle position and velocity.

Thirdly, even though there was no outlier and its initial states were accurate, localization could fall into the state ambiguities. As shown in Figure 11, the inverted moving direction and amplified angular velocity were observed with

the original CV model in *sine wave* and *square wave* trajectories. Non-zero acceleration in both trajectories is out of the assumption of CV or CSAV models, which might lead the state ambiguities. That is why orientation errors of the original models were quite higher than our expectation in Table 2. We also observed that the off-centered GPS observation model (+O) could resolve the state ambiguities.

Discussion With Outliers: Localization and velocity estimation errors *with* outliers and their example trajectories are described in Table 3, Figure 10, and Figure 12. These experiments with outliers aim to trigger more frequent state ambiguities (caused by outliers) and observe their recovery (facilitated by the proposed velocity constraints).

Firstly, the state ambiguities were more commonly observed in Table 3 because outliers trigger the state ambiguities. It is also more clearly visible in two sets of error distributions presented in Figures 9 and 10. Large orientation errors (e_o) indicate the inverted orientation shown in Figure 3b. Large angular velocity errors (e_w) indicate the extra spinning presented in Figure 3d. Even though outliers were generated at the middle of trajectories as 20% – 25%

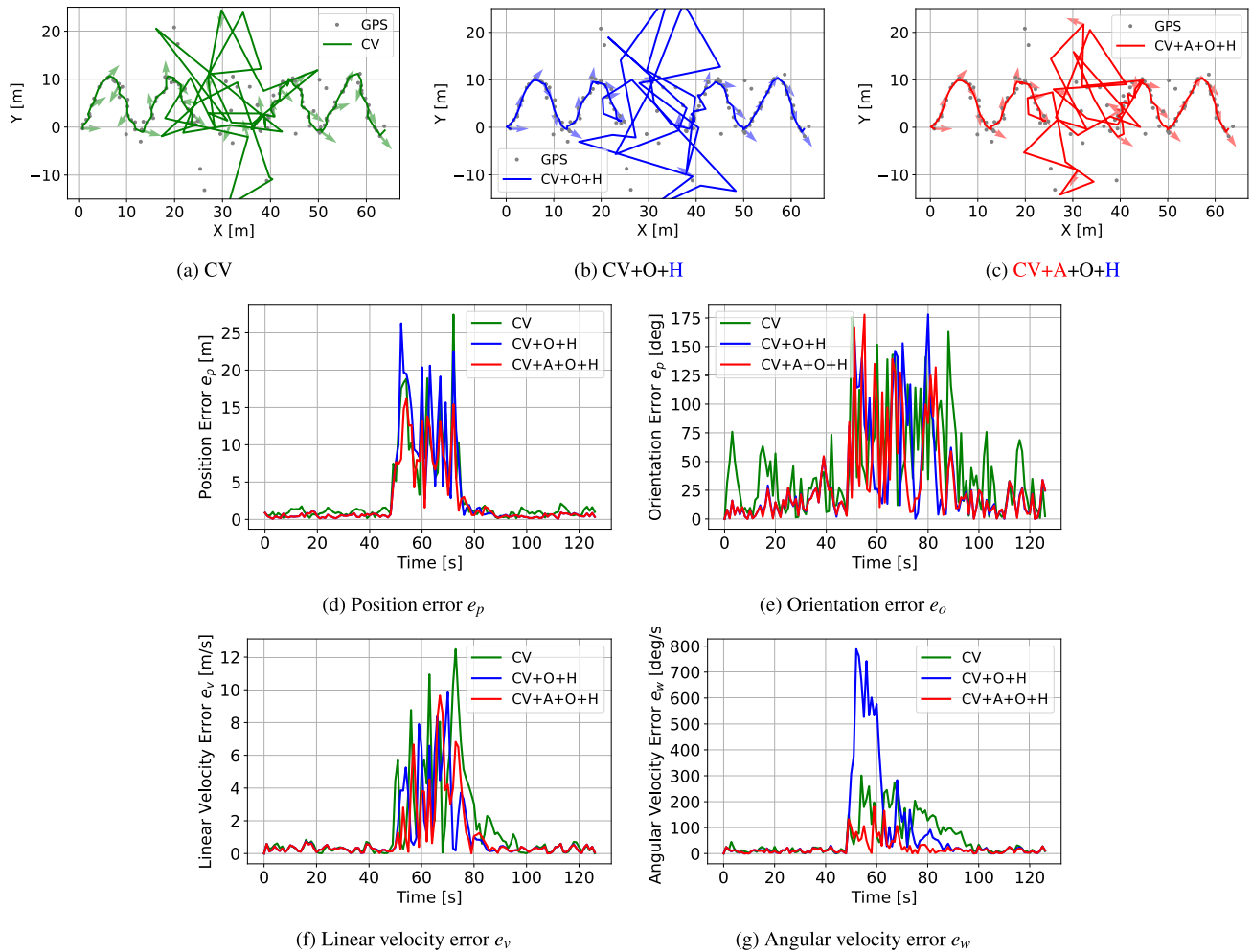


FIGURE 12. Localization and velocity estimation results on the sine wave trajectory with GPS data ($\sigma_G = 0.5$ meters and 1 Hz) with outliers.

of data, the state ambiguities were not recovered with normal GPS data. We used the median as a representative value, but the median values of errors (more than 50 percent of errors) were still quite large. It is also clear in Figure 10.

Secondly, the proposed method (CV+A+O+H) was the best, which is significantly better than the others. CV+A+O+H had 29%, 72%, 65%, and 94% less errors than the original CV model on average across all trajectories. In comparisons of CV and CV+A, the additional angular rate saturation significantly suppressed the angular velocity errors. However, CV+A still exhibited the state ambiguity regarding the unknown moving direction. In comparisons of CV+A+O and CV+A+O+H, the additional heading angle correction improved most categories of errors. These experimental results support why both velocity constraints are necessary together.

Thirdly, in contrast to Table 2, CSAV+O+H achieved the third-best accuracy. The CSAV motion model is an extreme situation of CV+A motion model with $w_{max} = 0$. It indicates that the angular rate saturation was highly effective in resolving the state ambiguities caused by outliers.

2) GPS NOISE AND FREQUENCY

We examined the effect of GPS noise and acquisition frequency on two velocity constraints. We performed experiments in all combinations of GPS noises (0.1, 0.2, 0.5, 1, 2, and 5 meters) and acquisition frequencies (1, 2, 5, and 10 Hz). These configurations spanned from highly accurate and responsive RTK-GPS systems to inaccurate and slow consumer-grade GPS systems. Each combination included 400 trials in total (100 times trials for each of the four trajectories).

Figures 13 and 14 present four error criteria *without* and *with* outliers, respectively. It was natural that higher GPS noise and less frequent GPS data (at the top-right) derived larger errors. Table 2 and 3 are located at the top-middle ($\sigma_G = 0.5$ meters and 1 Hz).

Firstly, we could find an important characteristic of the proposed method: its effectiveness was more relevant in more challenging situations (higher noise and less frequent data). The accuracy differences shown in the last row of Figure 13 indicate blue-colored improvements at the top-right. Such more difficult situations correspond to consumer-grade GPS systems.

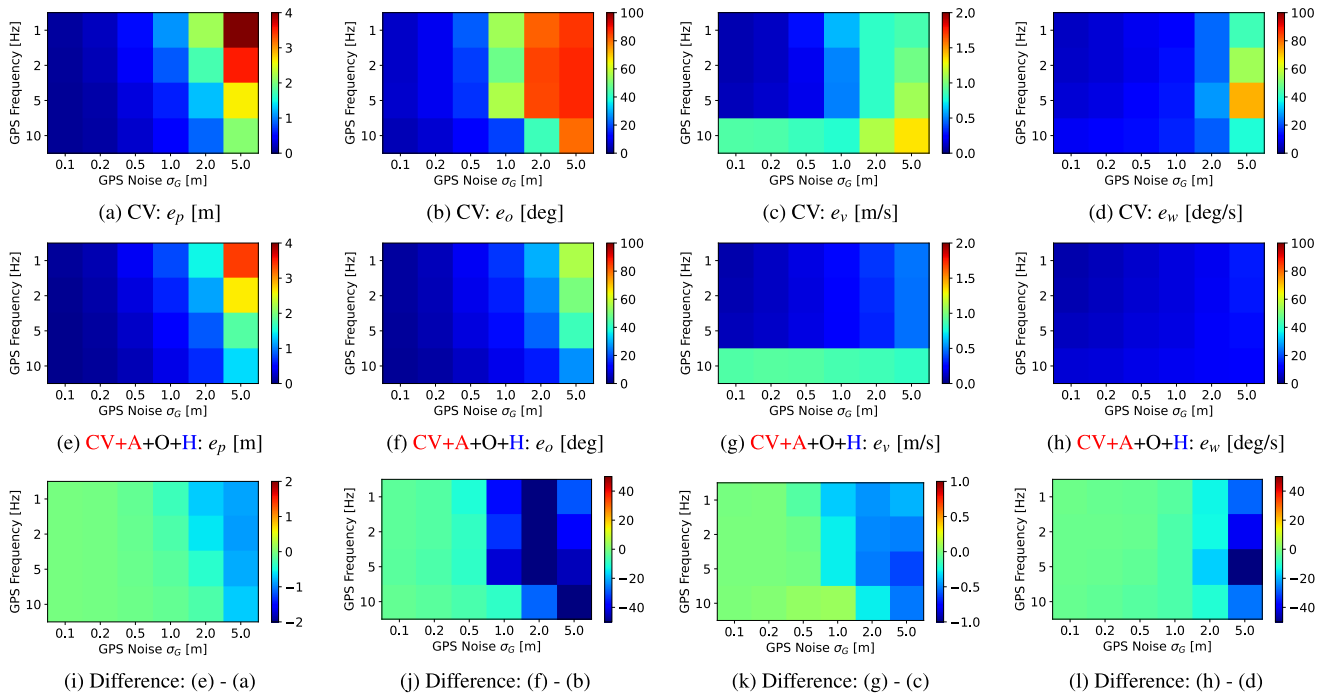


FIGURE 13. Localization and velocity estimation errors on all types of trajectories with varying GPS noise and GPS frequency *without* outliers: Lower (blue) is better. Higher (red) is worse.

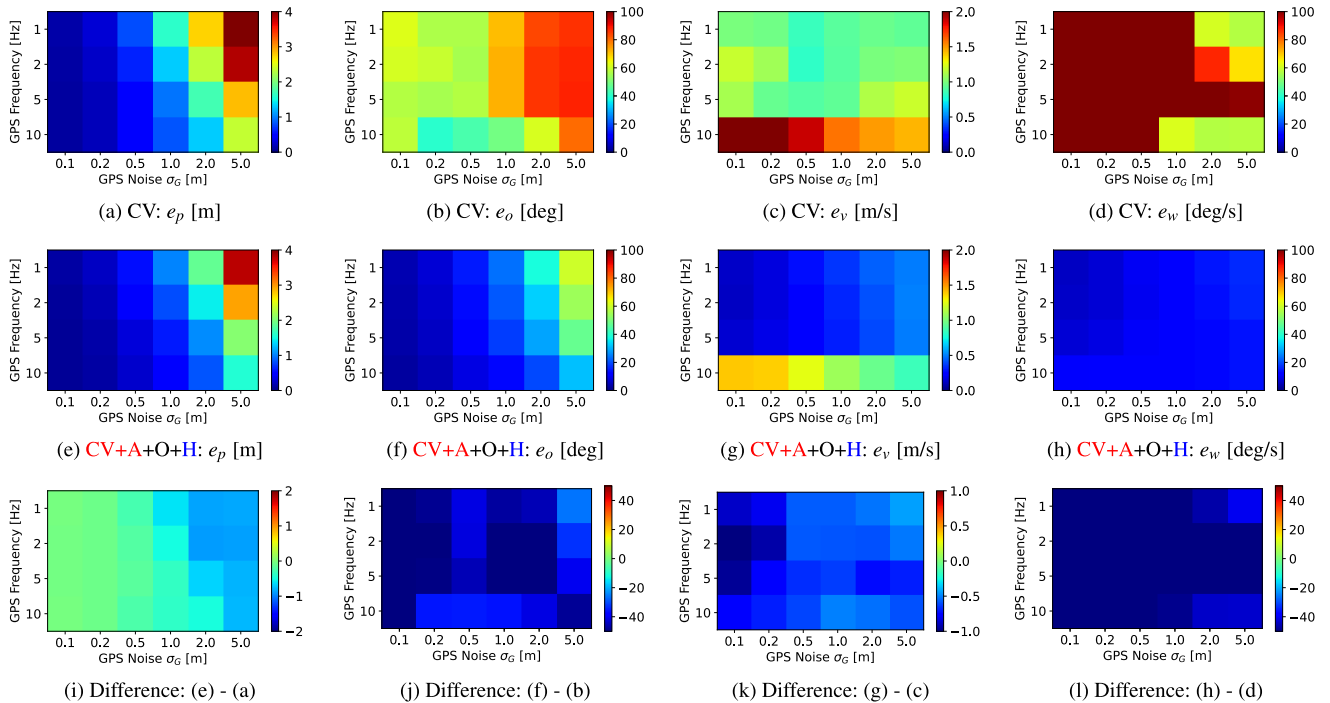


FIGURE 14. Localization and velocity estimation errors on all types of trajectories with varying GPS noise and GPS frequency *with* outliers: Lower (blue) is better. Higher (red) is worse.

Secondly, we could also observe that the proposed method was particularly beneficial in situations with outliers. as presented in the last row of Figure 14, the accuracy of orientation, linear, and angular velocities were consistently enhanced

across all combinations of GPS noises and frequencies. Outliers might raise state ambiguities more frequently and severely. The proposed method with two velocity constraints can effectively recover such state ambiguities.



FIGURE 15. The DRB autonomous track loader with an RTK-GPS whose antenna was attached at its vertical chassis due to its convenience of installation.

V. EXPERIMENTS WITH REAL-WORLD DATASETS

We conducted qualitative comparison *without* and *with* the proposed velocity constraints in two real datasets. Since the real data do not contain the true position, we analyzed their results qualitatively, rather than quantitatively.

A. DRB LOADER DATASET

1) CONFIGURATION

Our DRB Loader dataset comprised GPS data acquired from the DRB autonomous track loader based on *CAT 259D*. The track loader was equipped with an RTK-GPS, *SOKKIA GRX2*, operating at the GPS frequency of 1 Hz. The RTK-GPS was installed at $o_\rho = 1.166$ meters and $o_\phi = 30$ degrees from the center of the track loader due to the convenience of its mechanical attachment at the vertical chassis. The GPS data was obtained on an off-road circuit whose size was roughly 70×30 meters. The track loader with its GPS on the outdoor circuit is presented in Figure 15. The track loader ran the circuit three times. The GPS data contained position data in RTK mode and also in normal (also known as *single*) mode due to nearby terrain obstruction. During the beginning of first run, GPS data were not available due to signal blockage with the longest blockage lasting 5 seconds. GPS noise was configured as $\sigma_G = 0.5$ meters, and motion noise was set to $\sigma_v = \sigma_w = 0.1$ for optimal performance.

2) RESULTS AND DISCUSSION

Figure 16 presents localization and velocity estimation results by three localization methods on the DRB Loader dataset. It includes three trajectories with color visualizations of their angular velocities. Additionally, it contains three more plots showing orientation and velocity estimates over time. Figures 16d, 16e, and 16f clearly show the signal blockages and broken state estimates between 10 to 50 seconds.

As a result, the original CV model performed significantly worse than CV+O+H and CV+A+O+H models. The original CV model exhibited inaccurate position and the diverged angular velocity during signal blockages as shown

as orange-colored lines in Figure 16a. Moreover, while experiencing the state ambiguities, the original CV model also had unstable and inaccurate estimates of orientation and linear velocities presented in Figures 16d and 16e. It was an important observation that such intermittent signal blockages could also lead the state ambiguities. The original CV model recovered its state after approximately 60 seconds. We thought that such recovery might result from the very small GPS noise of the RTK-GPS system. As shown in our experiments with the synthetic dataset (Figures 13), the original CV model with small GPS noise also performed similarly to the our proposed constraints.

In contrast, CV+O+H and CV+A+O+H models had almost similar results. These observations were consistent with our experiments on synthetic dataset *without* outliers presented in Figure 11 and Table 2.

B. ETRI DEEPGUIDER DATASET

1) CONFIGURATION

The ETRI DeepGuider dataset [19] was recorded from an electric cart equipped with multi-modal sensors. We utilized its GPS data acquired from a consumer-grade GPS, *Ascen Korea GPS620*, operating at 1 Hz. The GPS antenna was installed at the front of the cart with offsets $o_\rho = 1$ meter and $o_\phi = 0$ degree. Its trajectory was approximately 2,000 meters long and included a dead zone due to nearby tall buildings. The dead zone was presented in Figure 17 as gray-colored boxes. The original trajectory of the cart was mostly going straight, but the GPS data in the dead zone were shifted to the north with higher values of variance. GPS noise was configured as $\sigma_G = 1$ meter, and motion noise was set to $\sigma_v = \sigma_w = 1$ for optimal performance.

2) RESULTS AND DISCUSSION

Figure 17 demonstrates localization and velocity estimation results by three methods on the ETRI DeepGuider dataset. Similarly, it includes six plots: three trajectories and three more plots showing orientation and velocity estimates over time. Figures 17a, 17b, and 17c shows the dead zone as gray-colored boxes at (700, 200) meters. We can also observe the corresponding dead zone (unstable orientations and linear velocities) in Figures 17d, 17e, and 17f between 19 to 22 minutes.

As a result, the original CV and CV+O+H models fell into the state ambiguities starting from 18 minutes. Figures 17a, 17b, and 17f exhibited amplified angular velocities. Two methods could not recover their overestimated angular velocities until the end. Moreover, Figure 17e also presents the backward motion (negative linear velocities) of the original CV model from 18 minutes. It was also not restored until the end.

In contrast, the CV+A+O+H model did not experience the state ambiguities. Only difference between CV+O+H and CV+A+O+H models is the utilization of the angular rate saturation. It revealed the importance of the angular rate

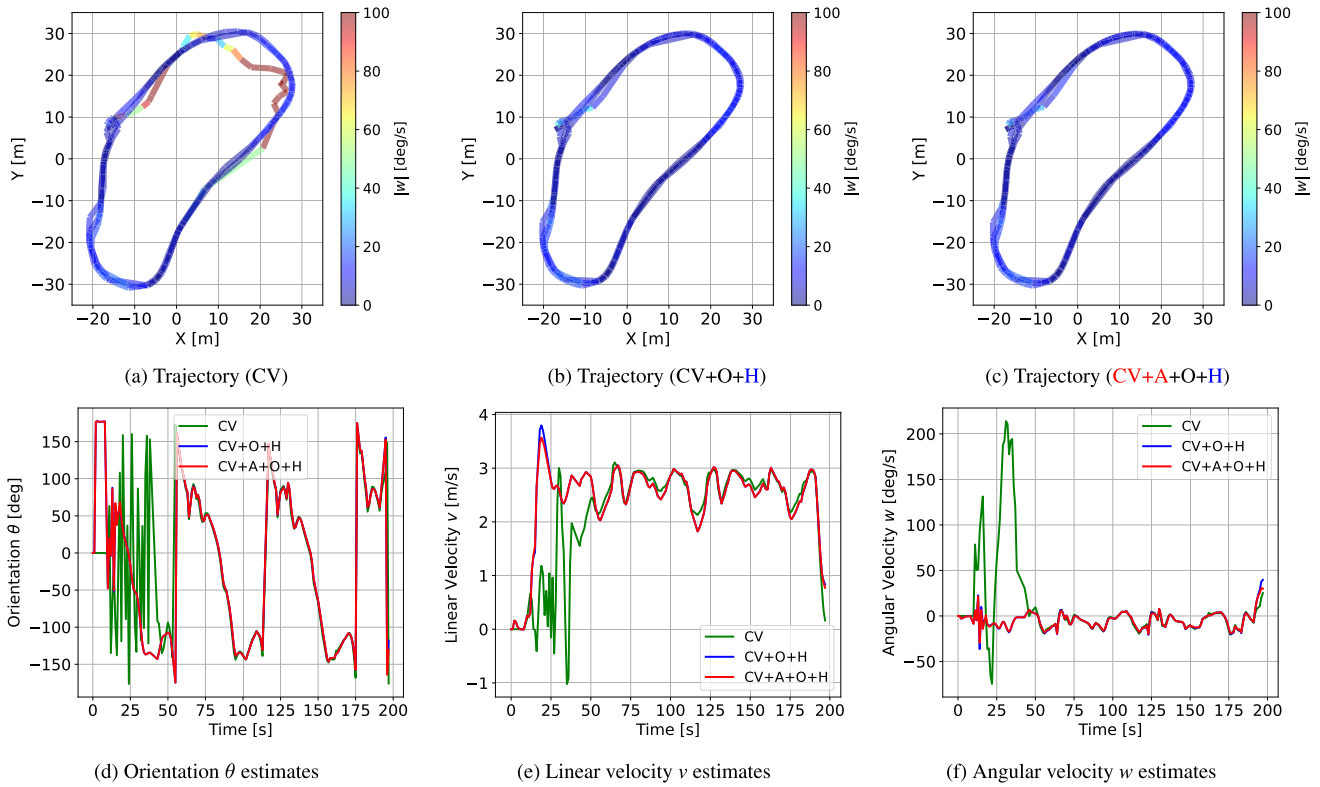


FIGURE 16. Localization and velocity estimation results with the *DRB Loader* dataset ($\sigma_G = 0.5$ meters and 1 Hz): Three trajectory figures (a), (b), and (c) also visualize the magnitude of angular velocity as the *jet* colormap.

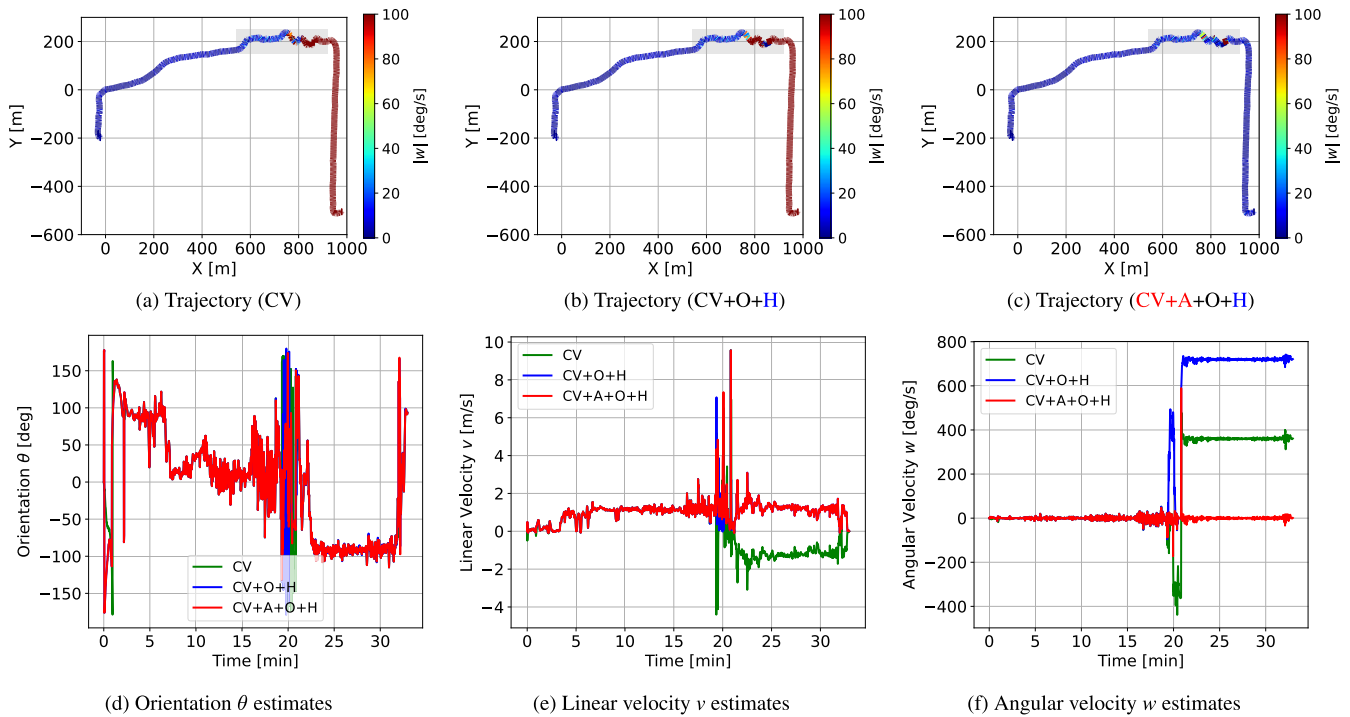


FIGURE 17. Localization and velocity estimation results with the *ETRI DeepGuider* dataset ($\sigma_G = 1$ meter and 1 Hz): Its GPS data were significantly inaccurate and biased at the dead zone (a gray-colored box at (700, 200) meters) due to nearby tall buildings. Three trajectory figures (a), (b), and (c) also visualize the magnitude of angular velocity as the *jet* colormap.

saturation to prevent the state ambiguities. Our additional experiments showed that other combinations of CV+A and

CSAV models without heading angle correction also avoided the state ambiguities.

VI. CONCLUSION

This paper proposed two velocity constraints for more accurate and resilient GPS-only localization. Since GPS-only localization inherently has the state ambiguity problem, its state estimates can be degraded (or ambiguous) when assumptions of motion and observation models are broken (e.g. abrupt rotation and outliers). Our heading angle correction can resolve the ambiguity of heading angle and linear velocity. Our angular rate saturation can suppress the incorrectly amplified angular velocity. In the framework of EKF localization, we demonstrated the effectiveness of these constraints with synthetic data and two real datasets. In the synthetic data, our proposed method with two velocity constraints (CV+A+O+H) achieved the best accuracy among all nine combinations. It achieved approximately 25% less position error and 70% less orientation error on average compared to the original CV model. Additionally, we could qualitatively observe the similar effectiveness in two real datasets. Two velocity constraints could avoid the scale ambiguities even though there were long signal blockages (in the DRB Loader dataset) and outliers (in the ETRI DeepGuider dataset).

In this paper, our problem formulation was 2D GPS-only localization, but our idea can be extended to 3D GPS-only localization. In three-dimensional spaces, linear and angular velocities are represented as three-dimensional vectors such as $[v_x, v_y, v_z]^T$ and $[w_x, w_y, w_z]^T$. When the frontal direction of a vehicle is a local X-axis, v_x is still a key to check the moving direction of a vehicle for the heading angle correction. Moreover, a hyperbolic tangent function can be applied to w_x , w_y , and w_z for the angular rate saturation. For ground vehicles, the maximum angular velocities for w_x (roll motion) and w_y (tilt motion) might be assigned smaller than the maximum of w_z (yaw motion).

We believe that our velocity constraints can be applied not only in Bayesian filtering but also in optimization approaches. As further work, we would like to extend our idea to develop more accurate 3D GPS-only localization using factor graph optimization and raw GPS data. Since these constraints were more beneficial in higher GPS noise and lower GPS frequency, we believe that our proposed ideas can be more practically applied to consumer-grade GPS systems.

REFERENCES

- [1] H. Aly, A. Basalamah, and M. Youssef, "Accurate and energy-efficient GPS-less outdoor localization," *ACM Trans. Spatial Algorithms Syst.*, vol. 3, no. 2, pp. 1–31, 2017.
- [2] X. Wei, J. Li, K. Feng, D. Zhang, P. Li, L. Zhao, and Y. Jiao, "A mixed optimization method based on adaptive Kalman filter and wavelet neural network for INS/GPS during GPS outages," *IEEE Access*, vol. 9, pp. 47875–47886, 2021.
- [3] S. Nirjon, J. Liu, G. DeJean, B. Priyantha, Y. Jin, and T. Hart, "COIN-GPS: Indoor localization from direct GPS receiving," in *Proc. 12th Annu. Int. Conf. Mobile Syst., Appl., Services (MobiSys)*, 2014, pp. 301–314.
- [4] Richard D. J. van Nee, "The multipath estimating delay lock loop," in *Proc. IEEE 2nd Int. Symp. Spread Spectr. Techn. Appl.*, Nov./Dec. 1992, pp. 39–42.
- [5] A. J. Van Dierendonck, P. Fenton, and T. Ford, "Theory and performance of narrow correlator spacing in a GPS receiver," *Navigation*, vol. 39, no. 3, pp. 265–283, Sep. 1992.
- [6] L.-T. Hsu, "Analysis and modeling GPS NLOS effect in highly urbanized area," *GPS Solutions*, vol. 22, no. 1, p. 7, 2017.
- [7] X. Qi, B. Xu, Z. Wang, and L.-T. Hsu, "Random forest-based multipath parameter estimation," *GPS Solutions*, vol. 28, no. 3, p. 126, 2024.
- [8] W. Wen and L.-T. Hsu, "Towards robust GNSS positioning and real-time kinematic using factor graph optimization," in *Proc. IEEE Int. Conf. Robot. Autom. (ICRA)*, May 2021, pp. 5884–5890.
- [9] A. V. Kanhere, S. Gupta, A. Shetty, and G. Gao, "Improving GNSS positioning using neural-network-based corrections," *Navigation*, vol. 69, no. 4, 2022, Art. no. navi.548.
- [10] X. Weng, K. Ling, and H. Liu, "PrNet: A neural network for correcting pseudoranges to improve positioning with Android raw GNSS measurements," *IEEE Internet Things J.*, vol. 11, no. 14, pp. 24973–24983, Jul. 2024.
- [11] P. Xu, G. Zhang, B. Yang, and L.-T. Hsu, "PositionNet: CNN-based GNSS positioning in urban areas with residual maps," *Appl. Soft Comput.*, vol. 148, Nov. 2023, Art. no. 110882.
- [12] D. Li, Y. Wu, and J. Zhao, "Novel hybrid algorithm of improved CKF and GRU for GPS/INS," *IEEE Access*, vol. 8, pp. 202836–202847, 2020.
- [13] Z. Z. M. Kassas, M. Maaref, J. J. Morales, J. J. Khalife, and K. Shamei, "Robust vehicular localization and map matching in urban environments through IMU, GNSS, and cellular signals," *IEEE Intell. Transp. Syst. Mag.*, vol. 12, no. 3, pp. 36–52, Fall. 2020.
- [14] J. Song, P. J. Sanchez-Cuevas, A. Richard, and M. Olivares-Mendez, "GPS-aided visual wheel odometry," in *Proc. IEEE 26th Int. Conf. Intell. Transp. Syst. (ITSC)*, Sep. 2023, pp. 375–382.
- [15] G. Cioffi and D. Scaramuzza, "Tightly-coupled fusion of global positional measurements in optimization-based visual-inertial odometry," in *Proc. IEEE/RSJ Int. Conf. Intell. Robots Syst. (IROS)*, Oct. 2020, pp. 5089–5095.
- [16] T. Shan, B. Englot, D. Meyers, W. Wang, C. Ratti, and D. Rus, "LIO-SAM: Tightly-coupled LiDAR inertial odometry via smoothing and mapping," in *Proc. IEEE/RSJ Int. Conf. Intell. Robots Syst. (IROS)*, Oct. 2020, pp. 5135–5142.
- [17] M. Dogramadzi and A. Khan, "Accelerated map matching for GPS trajectories," *IEEE Trans. Intell. Transp. Syst.*, vol. 23, no. 5, pp. 4593–4602, May 2022.
- [18] S. Sun, R. Sarukkai, J. Kwok, and V. Shet, "Accurate deep direct geo-localization from ground imagery and phone-grade GPS," in *Proc. IEEE/CVF Conf. Comput. Vis. Pattern Recognit. Workshops (CVPRW)*, Jun. 2018, pp. 1129–11297.
- [19] ETRI. *DeepGuider Dataset: Geo-Tagged Sidewalk Walking Sequences*. Accessed: Jun. 26, 2024. [Online]. Available: <https://nanum.etri.re.kr/share/rolicjy/deepguider>
- [20] T. Suzuki, "Time-relative RTK-GNSS: GNSS loop closure in pose graph optimization," *IEEE Robot. Autom. Lett.*, vol. 5, no. 3, pp. 4735–4742, Jul. 2020.
- [21] A. Mohanty and G. Gao, "Tightly coupled graph neural network and Kalman filter for smartphone positioning," in *Proc. Inst. Navigat. GNSS+ Conf. (ION GNSS+)*, 2023, pp. 175–187.
- [22] M. Kumar and S. Mondal, "Recent developments on target tracking problems: A review," *Ocean Eng.*, vol. 236, Sep. 2021, Art. no. 109558.
- [23] L. D. Stone, R. L. Streit, T. L. Corwin, and K. L. Bell, *Bayesian Multiple Target Tracking*. Norwood, MA, USA: Artech House, 2013.
- [24] D. N. Aloï and O. V. Korniyenko, "Comparative performance analysis of a Kalman filter and a modified double exponential filter for GPS-only position estimation of automotive platforms in an urban-canyon environment," *IEEE Trans. Veh. Technol.*, vol. 56, no. 5, pp. 2880–2892, Sep. 2007.
- [25] S. Choi and J.-H. Kim, "Leveraging localization accuracy with off-centered GPS," *IEEE Trans. Intell. Transp. Syst.*, vol. 21, no. 6, pp. 2277–2286, Jun. 2020.
- [26] K.-I. Na, S. Choi, and J.-H. Kim, "Adaptive target tracking with interacting heterogeneous motion models," *IEEE Trans. Intell. Transp. Syst.*, vol. 23, no. 11, pp. 21301–21313, Nov. 2022.
- [27] H. Chae, S. Choi, W. Yu, and J. Cho, "Autonomous navigation of mobile robot based on DGPS/INS sensor fusion by EKF in semi-outdoor structured environment," in *Proc. IEEE/RSJ Int. Conf. Intell. Robots Syst.*, Oct. 2010, pp. 1222–1227.

- [28] S.-F. Ch'ng, A. Khosravian, A.-D. Doan, and T.-J. Chin, "Outlier-robust manifold pre-integration for INS/GPS fusion," in *Proc. IEEE/RSJ Int. Conf. Intell. Robots Syst. (IROS)*, Nov. 2019, pp. 7489–7496.
- [29] Z. Zhou, H. Li, Z. Chen, and M. Lu, "Velocity consistency checking based GNSS spoofing detection method for vehicles," *IEEE Trans. Veh. Technol.*, vol. 73, no. 2, pp. 1974–1990, Feb. 2024.
- [30] T. Westny, J. Oskarsson, B. Olofsson, and E. Frisk, "Evaluation of differentially constrained motion models for graph-based trajectory prediction," in *Proc. IEEE Intell. Vehicles Symp. (IV)*, Jun. 2023, pp. 1–8.
- [31] M. J. Choi, Y. H. Kim, E. J. Kim, and J. W. Song, "Enhancement of heading accuracy for GPS/INS by employing average velocity in low dynamic situations," *IEEE Access*, vol. 8, pp. 43826–43837, 2020.
- [32] S. Habibi, "The smooth variable structure filter," *Proc. IEEE*, vol. 95, no. 5, pp. 1026–1059, May 2007.
- [33] Y. Li, G. Li, Y. Liu, X.-P. Zhang, and Y. He, "A novel smooth variable structure filter for target tracking under model uncertainty," *IEEE Trans. Intell. Transp. Syst.*, vol. 23, no. 6, pp. 5823–5839, Jun. 2022.
- [34] S. Akhtar, P. Setoodeh, R. Ahmed, and S. Habibi, "A new strategy for combining nonlinear Kalman filters with smooth variable structure filters," *IEEE Access*, vol. 11, pp. 146262–146281, 2023.
- [35] S. Thrun, W. Burgard, and D. Fox, *Probabilistic Robotics*. Cambridge, MA, USA: MIT Press, 2005.
- [36] NSTB/WAAS T&E Team (Satellite Navigation Branch), *Global Positioning System Standard Positioning Service Performance Analysis Report*, FAA William J. Hughes Tech. Center, Atlantic City International Airport, NJ, USA, Jan. 2021. [Online]. Available: https://www.nstb.tc.faa.gov/reports/2020_Q4_SPS_PAN_v2.0.pdf
- [37] F. van Diggelen and P. Enge, "The world's first GPS MOOC and worldwide laboratory using smartphones," in *Proc. 28th Int. Tech. Meeting Satell. Division Inst. Navigat. (ION GNSS+)*, 2015, pp. 361–369.



SE-HYOUNG CHO (Member, IEEE) received the B.S. degree in electric and electronic engineering from the University of Seoul, Republic of Korea, in 2004, and the M.S. degree in electric and electronic engineering and the Ph.D. degree in robotics from KAIST, Daejeon, Republic of Korea, in 2007 and 2016, respectively. From 2017 to 2023, he was an Assistant Professor with the Department of Information and Communications Technology, Sun Moon University, Republic of Korea. His research interests include autonomous navigation, humanoid robots, and reinforcement learning.



SUNGLOK CHOI received the B.S. degree in mechanical and aerospace engineering from Seoul National University, Seoul, Republic of Korea, in 2006, and the M.S. and Ph.D. degrees in robotics from KAIST, Daejeon, Republic of Korea, in 2008 and 2019, respectively. From 2008 to 2021, he was a Research Scientist with the Electronics and Telecommunications Research Institute (ETRI), Daejeon. Since 2021, he has been an Assistant Professor with the Department of Computer Science and Engineering, Seoul National University of Science and Technology (SeoulTech). His research interests include autonomous navigation, 3D computer vision, and robust regression.

• • •